Swarming in shallow waters

Swarming in shallow waters.

Siowling Soh[1], Michal Branicki[1,3] and Bartosz A. Grzybowski[1,2]*

[1]Department of Chemical and Biological Engineering, Northwestern University, 2145 Sheridan Road, Tech E-136, Evanston, IL 60208

[2]Department of Chemistry, Northwestern University, 2145 Sheridan Road, Evanston, IL 60208

[3]School of Mathematics, University of Bristol, University Walk, Bristol, BS8 1TW, UK

*To whom correspondence should be addressed:
E-mail: grzybor@northwestern.edu

Swarming is a unique manifestation of dynamic self-assembly (DySA)[1-3] in which self-propelling objects not only organize into dissipative structures but also perform collective motions. While swarms are ubiquitous in biological systems (bacteria[4,5], fish[6], ants[7,8], etc.), the examples of artificial collective movers are largely limited to complex robotics systems[9,10]. The chief difficulty in making simple components swarm is to engineer interactions that would propel these components while maintaining them at a distance from and in proper orientation with respect to one another. Here, we describe a hydrodynamic system in which swarming is mediated by asymmetric convection "rolls" around small, millimeter-sized gel particles floating at a water/air interface and emitting surface active chemicals. Remarkably, for thin water layers, these convective flows give rise to interparticle attractions that bring the particles close to – but not into contact – with one another. In collections of identical particles, this previously undescribed hydrodynamic interaction leads to the formation of high-symmetry, open-lattice, stationary structures. In contrast, particles of different shapes assemble into lower-symmetry, dynamic formations

that swarm around the interface. Our system provides a convenient experimental test bed with which to engineer and study collective and swarming behaviors.

Fabrication of the gel particles[11,12] used in this work began with standard photolithography in SU8 photoresist followed by molding into poly (dimethyl siloxane), PDMS. The PDMS master thus prepared presented millimeter sized, 1 mm deep wells, which defined particles' shapes. These wells were filled by a 5% w/w solution of hot agarose. After gelation, the particles were liberated from the master and were soaked in a saturated solution of camphor in methanol (1.1 g/mL) for several hours. Immediately prior to use, the particles were thoroughly rinsed with water to precipitate camphor inside their bulk and to remove any excess camphor on their surfaces. This process resulted in a uniform loading of solid camphor occluded in the gel pieces. These camphor-filled particles (commonly known as camphor boats[13-15]) were 1 mm thick and were placed on the air-water interface in a polystyrene Petri dish containing different volumes of water such that the thickness h of the water layer varied between 1.2 mm and 5 mm (Fig. 1a)

For $h > 1.8$ mm, the particles moved randomly around the interface and repelled one another through hydrodynamic interactions described in detail before[11]. In this regime, the particles did not form any stable, ordered structures. When, however, the thickness of the liquid layer was decreased to $h \sim 1.4 - 1.8$ mm, the particles formed open lattice structures such as those shown in Fig. 1 and 2 (also see Movie 1 in the Supporting Information, SI). When all the particles had the same shapes (e.g., rods in Fig. 1b or disks in Fig. 1c), the dynamic lattices were stationary. When, however, pieces of different shapes and low symmetries were present, the assemblies performed collective motions (Fig. 2). For example, when a small U-shaped particle

was added to a collection of disks or rods, it precessed around the aggregate, thus causing it to rotate (Fig. 2a and Movie 2 in the SI). On the other hand, if a V-shaped particle was larger, it "recruited" the smaller particles that swarmed in its wake. This is vividly illustrated in Fig. 2b (and Movie 3 in the SI) which shows six smaller, rod-shaped "followers" assembling and moving behind a larger, V-shaped "leader". An interesting observation here is that when the number of the "followers" was even, they divided equally behind the two arms of the "leader" and the swarm moved predominantly forward. When, however, their total number was odd (Fig. 2c and Movie 4 in the SI), the numbers of followers behind each arm differed by one and the entire assembly rotated. Also, when the depth of the fluid was lowered to ~ 1.6 mm, the "leader" reversed its direction of motion and pushed the followers organized in its front (Fig. 2d and Movie 5 in the SI). We emphasize that in all cases, the final structures and their behaviors did not depend on the initial locations of the particles on the interface but only on the value of h.

In addition to dynamic self-organization and swarming, the assemblies exhibited primitive forms of taxis: for instance, if the depth of the water layer was not uniform, they migrated toward shallow-water regions. In the presence of a temperature gradient, the assemblies moved towards warmer waters. We note that in all arrangements, the individual particles did not move (and hence, assemble) far fluid depth $h < 1.4$ mm, likely due to an increased drag force, F_D, which scales inversely with the distance, h, between the bottom surface of the particle and the surface of the Petri dish (see SI, Section 1).

Dynamic self-organization and swarming are due to hydrodynamic interactions between the particles (and not due to, for instance, capillarity[16], also see SI, Section 2). These interactions derive from a combination of surface tension gradients (due to surface-active camphor emitted

onto liquid-air interface) and the convective flows/rolls around the particles. We have previously showed that for deep waters (h large compared to the boat thickness), the convection rolls around the particles reflect particle symmetry and give rise to interparticle repulsions. In the present case, however, the water layer is thin, and the convective flows are affected by the bottom surface of the container – it is this "distortion" of the convective flows that modifies the nature of forces acting in the system from repulsive at small particle separations to attractive at longer separations.

To show this, we calculated the interparticle forces from the three-dimensional flow fields around the interacting particles. Specifically, we considered a model system of two proximal, parallel rods (3 mm x 1 mm x 1 mm) separated by distance, d (cf. Fig. 1a). For a given steady-state value of d, the flows are determined by the Navier-Stokes equation, $\rho \mathbf{v} \cdot \nabla \mathbf{v} = -\nabla P + \mu \nabla^2 \mathbf{v}$, combined with the continuity equation (assuming incompressibility of the fluid), $\nabla \cdot \mathbf{v} = 0$, and transport equation for camphor, $\mathbf{v} \cdot \nabla c = D \nabla^2 c$. In these equations, $\mathbf{v}$ stands for fluid velocity, P denotes pressure, μ is fluid viscosity, ρ is density, c is concentration of camphor, $D = 1 \times 10^{-9}$ m^2/s is camphor diffusivity[19], and boldface characters indicate vectors. At the air-water interface, $z = S$, spreading of camphor from the particles reduces the surface tension. The surface tension gradients thus created give rise to shearing stresses driving Marangoni-type convection rolls in the fluid. The tangential stresses imposed at the air-water interface are given by $\tau_{zx} = \partial \gamma / \partial x \big|_{z=S}$ and $\tau_{zy} = \partial \gamma / \partial y \big|_{z=S}$, where γ denotes surface tension. Since camphor is only sparingly soluble in water, the variation of surface tension with the concentration of camphor can be approximated as linear[17]: $\gamma = \gamma_o - bc$, where γ_o denotes surface tension of pure water (72 mN/m) and b = 0.003 N·m^2/mol as determined before[11]. This

approximation enables relating camphor concentration to shearing stresses at the interface as

$$\tau_{zx} = \mu\left[\frac{\partial v_z}{\partial x} + \frac{\partial v_x}{\partial z}\right]_{z=S} = \left.\frac{\partial \gamma}{\partial x}\right|_{z=S} = -b\left.\frac{\partial c}{\partial x}\right|_{z=S} \text{ and } \tau_{zy} = \mu\left[\frac{\partial v_y}{\partial z} + \frac{\partial v_z}{\partial y}\right]_{z=S} = \left.\frac{\partial \gamma}{\partial y}\right|_{z=S} = -b\left.\frac{\partial c}{\partial y}\right|_{z=S}.$$

Additionally, spreading of camphor at the air-water interface is accompanied by its sublimation which can be accounted for by the rate equation[15] $\partial c_S / \partial t = -kc_S$, where $k \sim 10^{-10}$ m/s is the rate of sublimation (see SI, Section 3) . Since the z-component of fluid velocity at the interface is zero (at steady state), the sublimation is equal to the diffusive flux of camphor from the bulk fluid: $-D\partial c / \partial z\big|_S = kc_S$. On the surfaces of the particles, the boundary conditions are no-slip for the velocity field and constant, saturated concentration, c_0 (~ 8 mM[18]) of camphor for the transport equation. The boundary conditions imposed on the dish walls are no-slip for the velocity field and no flux of camphor across the walls. When the equations were solved numerically using Fluent Computational Fluid Dynamics software (from Ansys, Inc.), the magnitude of the net force acting on each particle in the horizontal direction x, connecting the geometric centers of the particles, could be calculated as a sum of pressure, $F_p = \mathbf{e}_x \cdot \int_W P\mathbf{n}_W dW$, and viscous, $F_v = \mathbf{e}_x \cdot \int_W \boldsymbol{\tau}\mathbf{n}_W dW$ contributions, where W represents all the submerged surfaces of the particle, $\boldsymbol{\tau}$ is the viscous part of the stress tensor, $\mathbf{e}_x$ is the unit vector pointing in the x direction, and $\mathbf{n}_W$ is the unit vector normal to the surface of the particle.

Figures 3a and 3b show the calculated net force acting on each particle as a function of particle separation, d, for two fluid depths, h = 1.8 mm and h = 1.4 mm. For the deeper layer, the interaction is purely repulsive ($F_p + F_v > 0$); for the thinner layer, however, the force changes from repulsive to attractive at d_{eq} = 2.3 mm corresponding to a stable particle configuration.

When performed for different fluid depth, the calculations give a phase diagram in Fig. 3c where the predicted interparticle separations d_{eq} (blue line) agree well with the values observed experimentally (red markers).

The nature of the forces can be qualitatively described as follows. Repulsive forces between two sufficiently proximal particles are due to the fact that camphor gradients are shallower in the region "between" the particles than in the region "outside" of them (Fig. 3d), leading to larger shearing stresses on the "outside". In deep waters, these large shearing stresses cause convective rolls to rise almost vertically near the particle and then rapidly flow outward near the surface of the fluid (Fig. 3e). These rapid outflows translate into the pressure being lower on the "outside" than "between" the particles. On the other hand, in shallow waters, the convective rolls are distorted by the bottom of the dish, such that the "return" flows converging back toward the particles are mainly perpendicular to the particles' side walls (Fig. 3f). These backflows exert pressure on the side walls of the particles, effectively pushing them toward each other. This "pushing" is opposed by the force due to surface flows "between" the particles – when balanced, these effects result in stable particle configuration at a non-zero particle-particle distance, d_{eq}.

The model also explains the behavior of V-shaped particles leading the swarms (cf. Fig. 2). These particles create asymmetric concentration profiles of camphor and, consequently, asymmetric flows around themselves (Fig. 4). Specifically, concentration gradients are steeper and the shearing stresses are larger around the spiked "front" of the particle than near its wide "rear". In deep waters, these large shearing stresses drive convective rolls that rise nearly vertically near the particle and then "jet" outwards (Fig. 4a) creating a low pressure region "in

front" of the particle – hence, the particle moves pointed-end first. In shallow waters, however, the convection rolls are affected and distorted by the bottom of the dish such that the backflows have appreciable component perpendicular to the particle's side walls. These backflows exert pressure on the side walls and cause the particle to move wide-end first (Fig. 4b). Remarkably, calculations predict the direction of motion to change at the fluid depth $h \approx 1.67$ mm compared to 1.6 mm observed experimentally. Finally, we note that since the concentration profile and flow field are influenced mostly by the large V-shaped particle, the overall flow pattern of the assembly, in general, resembles that of the large "leader", which directs the collective motion of the particles.

In summary, we described a system in which hydrodynamic interactions drive the formation of swarms of millimeter-sized particles. The singular feature of this system is that by adjusting the particle shapes, the collective behaviors of the particles can be controlled. In this way, and with the help of fluid-mechanical models, different types of swarms can be engineered rationally. Our system – and others similar to it – constitute a convenient test-bed for studying dynamic self-assembly[1-3] and collective behaviors in non-equilibrium systems.

References:

1. Whitesides, G. M. & Grzybowski, B. Self-assembly at all scales. *Science* **295**, 2418-2421 (2002).
2. Camazine, S. *et al.*, *Self-organization in biological systems*. (Princeton University Press, Princeton, 2003).
3. Fialkowski, M. *et al.* Principles and implementations of dissipative (dynamic) self-assembly. *J. Phys. Chem. B* **110**, 2482-2496 (2006).
4. Fraser, G. M. & Hughes, C. Swarming motility. *Curr. Opin. Microbiol.* **2**, 630-635 (1999).
5. Budrene, E. O. & Berg, H. C. Complex patterns formed by motile cells of escherichia-coli. *Nature* **349**, 630-633 (1991).
6. Okubo, A. Dynamical aspects of animal grouping: Swarms, schools, flocks, and herds. *Adv. Biophys.* **22**, 1-94 (1986).
7. Bonabeau, E., Dorigo, M., & Theraulaz, G. Inspiration for optimization from social insect behaviour. *Nature* **406**, 39-42 (2000).
8. Deneubourg, J. L. & Goss, S. Collective patterns and decision-making. *Ethol. Ecol. Evol.* **1**, 295-311 (1989).
9. Mondada, F. *et al.* Swarm-bot: A new distributed robotic concept. *Auton. Robot.* **17**, 193-221 (2004).
10. Martinoli, A., Easton, K., & Agassounon, W. Modeling swarm robotic systems: A case study in collaborative distributed manipulation. *Int. J. Robot. Res.* **23**, 415-436 (2004).
11. Soh, S., Bishop, K. J. M., & Grzybowski, B. A. Dynamic self-assembly in ensembles of camphor boats. *J. Phys. Chem. B* **112**, 10848-10853 (2008).

12. Wesson, P. J. *et al.* "Remote" Fabrication via three-dimensional reaction-diffusion: Making complex core-and-shell particles and assembling them into open-lattice crystals. *Adv. Mater.* **21**, 1911-1915 (2009).

13. Nakata, S. *et al.* Self-rotation of a camphor scraping on water: New insight into the old problem. *Langmuir* **13**, 4454-4458 (1997).

14. Kohira, M. I., Hayashima, Y., Nagayama, M., & Nakata, S. Synchronized self-motion of two camphor boats. *Langmuir* **17**, 7124-7129 (2001).

15. Kitahata, H. *et al.* Self-motion of a camphor disk coupled with convection. *Phys. Chem. Chem. Phys.* **6**, 2409-2414 (2004).

16. Grzybowski, B. A. *et al.* Modeling of menisci and capillary forces from the millimeter to the micrometer size range. *J. Phys. Chem. B* **105**, 404-412 (2001).

17. Adamson, A. W., *Physical chemistry of surfaces*, 6th ed. (Wiley, New York, 1997).

18. *The Merck index*, 14 ed. (Merck, New Jersey, 2006).

Figure Captions:

Figure 1 | a, Scheme of the system comprising camphor-soaked particles (here, two rods) floating at the interface between water and air. The arrows illustrate the convective flows created around the particles by the outflow of surface-active camphor. **b** and **c,** show typical, open-lattice assemblies of, respectively, rod-shaped and disk-shaped particles for water depth h ~1.4 – 1.8 mm. Dimensions for rods are 3 mm × 1 mm × 1 mm and disks are 1 mm in diameter and 0.5 mm thick. Scale bars = 1 cm.

Figure 2 | Swarming in assemblies comprising particles of different shapes. **a,** Introduction of a smaller, U-shaped particle into a stationary assembly of rods causes overall rotation of the ensemble. **b,** When a much larger asymmetric V-shaped particle is added to an even-numbered (here, six) collection of rods, the whole assembly swarms directionally, with the V-shaped particle acting as the leader. **c,** When the assembly comprises an odd number of rods (here, five rods) it moves forward and also rotates. **d,** For very thin fluid layers, the V-shaped particle reverses its direction of motion and instead of "leading" the rods, it pushes them in front of itself. Experimental times (in seconds) are shown on each image. The fading blue markers outline the past trajectory of the assembly and the arrows indicate the direction of rotation. Movies 2 – 5 in the SI accompany the images shown. Scale bar for (**a**) = 2 mm. Scale bars for (**b**) – (**d**) = 1 cm.

Figure 3 | Origins of repulsive and attractive interactions between two camphor-filled particles. a and b, Plots of the calculated viscous, pressure and net forces as a function of particle separation, d, for water depth, h = 1.8 mm and h = 1.4 mm (particle thickness is 1 mm in both cases). Positive values correspond to repulsive forces. The net force is always repulsive for deeper waters. In shallow waters, however, the force is repulsive for small d and attractive for

large d. **c,** The stable distance, d_{eq} (when there is no net force on the particle), varies with h. Results from the model (blue line) agree well with experiments (red markers). **d,** Modeled concentration profile at the air-water interface for h = 1.8 mm, illustrating shallower concentration gradient in the region "between" the particles than "outside" of them. **e** and **f,** illustrate the 3D flow structure around the particles for high and low water levels, respectively. For deeper water layers, the flows are roughly tangential to the side walls of the particles and the rapid outflow creates low pressure around the particles resulting in their repulsion. In shallow waters, the bottom of the dish distorts the backflow, such that it is mostly perpendicular to the side walls of the particles, hence, "pushing" them together and resulting in particle attraction.

Figure 4 | Forward and backward motion of a V-shaped particle at different water depths. **a,** For sufficiently deep water layer, large shearing stresses at the spiked "front" of the particle create low pressure therein driving the particle forward (red arrow). **b,** In shallow waters, the bottom of the dish distorts the convective "backflows", such that they impinge roughly perpendicularly onto the vertical walls of the particle. The pressure thus exerted causes the particles to move wide-end first **c,** A simulated concentration profile of camphor at the air-water interface for h = 1.6 mm. Due to the asymmetric geometry, the concentration gradient in front of the particle is steeper than at its rear, resulting in larger shearing stresses in front, as illustrated in (**a**). **d,** Calculated forces acting on the particle at varying depths of water, h. If $F_{net} > 0$ (for $h >$ 1.67 mm), the particle moves spiked-end first, as in (**a**); if $F_{net} < 0$ (for $h <$ 1.67 mm), the particle moves wide-end first. The predicted transition between the two modes of motion at $h \approx$ 1.67 mm, is close to 1.6 mm observed in experiments.

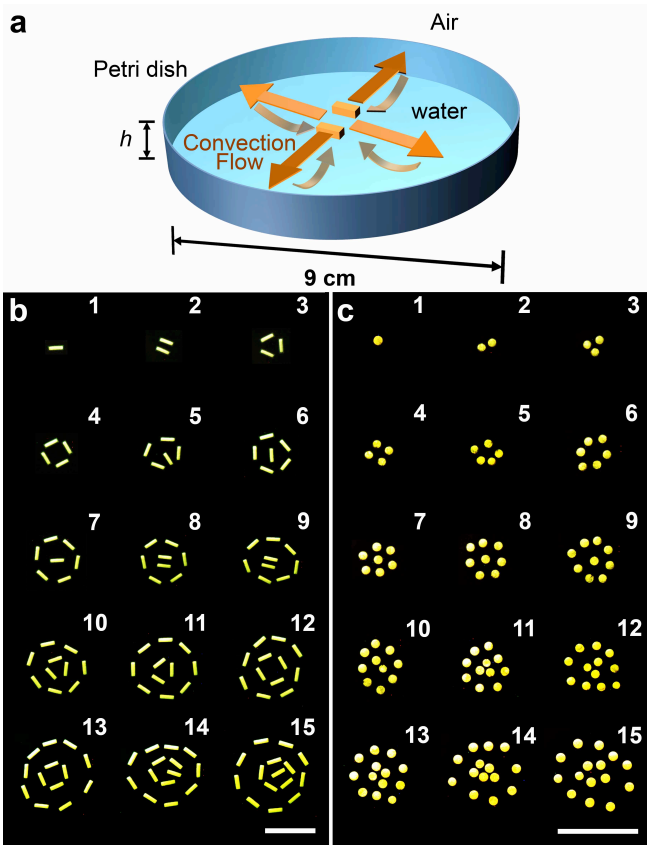
a
Air
Petri dish
water
h
Convection
Flow
9 cm
b
c
1
2
3
4
5
6
7
8
9
10
11
12
13
14
15

Figure 1

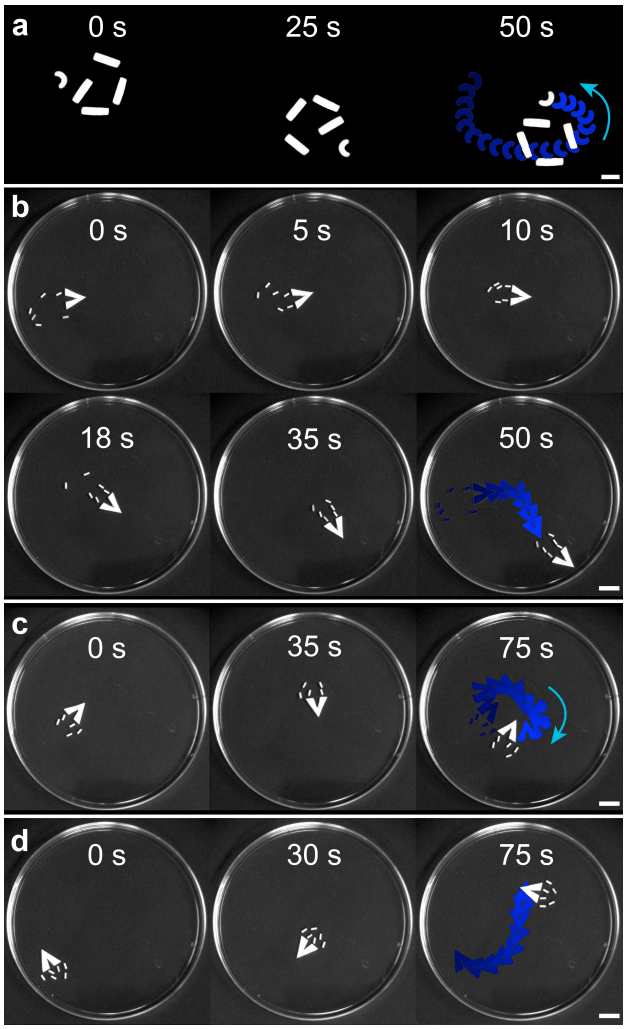

Figure 2

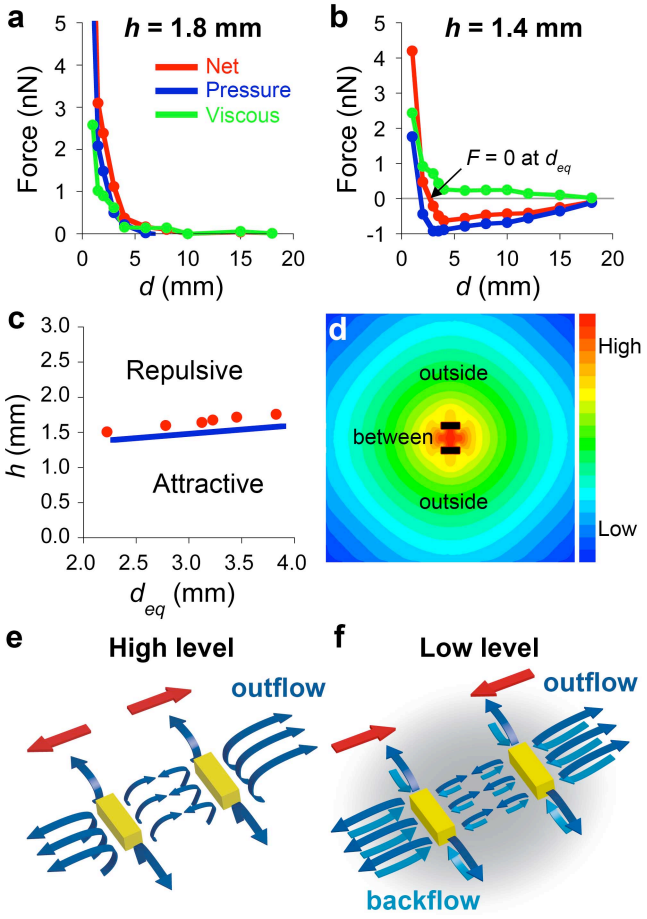
a
h = 1.8 mm
Net
Pressure
Viscous
Force (nN)
d (mm)
b
h = 1.4 mm
F = 0 at d_eq
Force (nN)
d (mm)
c
Repulsive
Attractive
h (mm)
d_eq (mm)
d
outside
between
outside
High
Low
e
High level
outflow
f
Low level
outflow
backflow

Figure 3

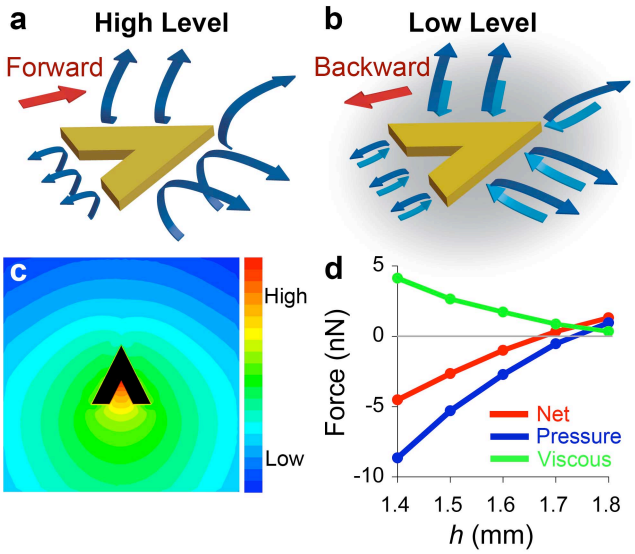
a
High Level
Forward
b
Low Level
Backward
c
High
Low
d
5
0
-5
-10
Force (nN)
Net
Pressure
Viscous
1.4
1.5
1.6
1.7
1.8
h (mm)

Figure 4

Supplementary Information for Manuscript entitled "*Swarming in shallow waters*" by S. Soh, M. Branicki and B.A. Grzybowski*

1. Drag force between bottom surface of a particle and the surface of the Petri dish

As narrated in the main text, for sufficiently thin water layers (h < 1.4 mm), there is little, if any, motion of the particles, even though they are not in contact with the base of the Petri dish (height of particles is 1 mm). This "stalling" can be rationalized by considering the drag exerted on the bottom of the boat by a thin layer (thickness h, Fig. S1) of fluid separating it from the surface of the dish.

Figure S1 | Scheme illustrating the velocity profile within the thin fluid layer between the bottom surface of the particle and the surface of the Petri dish.

Specifically, approximating the flow as a simple unidirectional flow between a moving plate (bottom surface of the particle) and a stationary plate (Petri dish; Fig. S1), the Navier-Stokes equations reduce to $\frac{d^2 v_x}{dz^2} = \frac{1}{\mu}\frac{dP}{dx}$, where v_x denotes horizontal velocity, μ is viscosity and P is pressure. Assuming that the pressure drop is constant (which is exactly true for flow between infinite plates) and together with the boundary conditions, $v_x = U$ at $z = h$ and $v_x = 0$ at $z = 0$, this

equation is easily solved to give $v_x = \frac{1}{2\mu}\frac{dP}{dx}\left(z - h\right)z + \frac{U}{h}z$. The drag force acting on the bottom of the particle is obtained by evaluating: $F_D = \mu \left.\frac{\partial v_x}{\partial z}\right|_{h} A_{bottom}$, where A_{bottom} is the surface area of the bottom of the particle. Substituting for v_x gives $F_D = \left(\frac{1}{2}\frac{dP}{dx}h + \frac{\mu U}{h}\right)A_{bottom}$. For small h, this expression is approximately $F_D \approx \mu U A_{bottom} / h$, giving the scaling relationship $F_D \sim 1/h$. In other words, the drag force resisting particle's motion due to surface-tension effects becomes increasingly important as h decreases. We note that the above analysis, in which the particle's bottom is assumed to be parallel to the surface of the dish, does not take into account the stability of such a configuration. Additional effects may become important in a more realistic case when the angle of inclination with respect to the bottom of the dish is allowed to vary. More detailed discussion of these effects can be found in, for example, Ref. S1.

2. Potential influence of capillarity.

In principle, attraction between the particles could be caused by capillary interactions due to the menisci forming between the particles[S2,S3] or by buoyancy effects which prevail over the "capillary suction" for sufficiently small particles[S4]. However, direct imaging of the interface (along it plane, using high-resolution camera) shows no appreciable menisci around the particles in either deep or shallow waters. Most importantly, we performed experiments in which either hydrophobic or hydrophilic particles (not soaked with camphor) were placed at the interface along with the camphor-soaked boats. If capillarity were at play, one type of these particles

should be attracted to the boats, and the other, repelled (Fig. S2). In reality, both types of particles are drawn toward the boats by the surface-tension-driven flows.

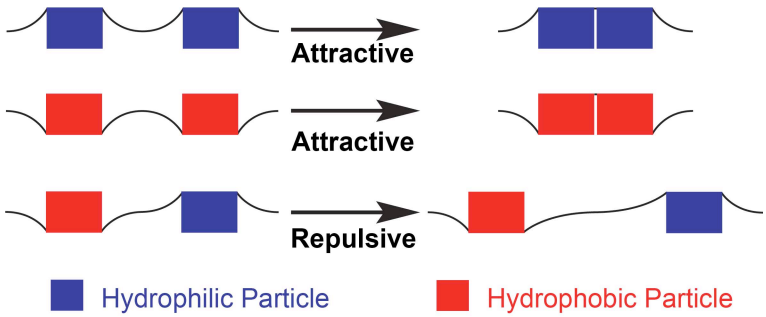

Figure S2 | Illustrations of capillary forces acting between hydrophilic and hydrophobic particles. If the particles are of the same "type," (i.e., hydrophilic-hydrophilic or hydrophobic-hydrophobic), the particles attract one another. However, if the particles are of different "types" (i.e., hydrophobic-hydrophilic), the particles repel.

3. Estimation of the rate of sublimation, k

As camphor spreads on the interface around the particles, it also sublimates. The rate of sublimation, k, can be estimated experimentally from the time needed to sublimate all the camphor initially stored in the gel particle. In a typical experimental setup, a cylindrical gel particle (1 mm in diameter, 0.5 mm thick) was placed in a Petri dish (12 cm diameter), where motion of the particle normally persists for $t_{expt} \sim 2$ hours. Prior to use, the particle was soaked in a saturated solution of camphor-in-methanol for several hours. Since the mass of agarose in the particle was only 5%, the volume of methanol contained in the gel was close to the volume of the particle ($\sim 4 \times 10^{-10}$ m^3). The amount of camphor, m_c, stored in the gel can be calculated from the saturated concentration of camphor in methanol (1.1 g/mL) giving 10^{-4} g or 10^{-7} mol (molecular weight of camphor is 152 g/mol).

Knowing the amount of camphor initially stored in the gel particle, it is possible to calculate the flux, f, (with units mol/m^2·s) of camphor onto the interface for the total duration of $t_{expt} \sim 2$ hours. The area of the air-water interface is $A_I = 10^{-2}$ m^2 for a dish of 12 cm in diameter. The flux can be estimated using $f \sim m_c / \left(A_I \times t_{\exp t} \right)$, giving $f \sim 10^{-9}$ mol/ m^2·s.

This flux is related to k by assuming a first-order rate of sublimation as mentioned in the main text : $f = -kc_S$, where c_S is the concentration of camphor at the interface. Since spreading of camphor is strongly aided by convection, we assume here that the concentration of camphor in water is near saturation at 8 mM (verified later by concentration profiles from simulation). This means that $f \sim -kc_{Saturation}$, where the rate of sublimation is estimated to be $k \sim 10^{-10}$ m/s.

Supplementary References:

S1. Michell, A.G.M., *Lubrication: Its Principles and Practice*, Blackie and Son Ltd., London 1950.

S2. Bowden, N., Terfort, A., Carbeck, J. & Whitesides, G.M. Self-assembly of mesoscale objects into ordered two-dimensional arrays. *Science* **276**, 233-235 (1997).

S3. Grzybowski, B.A., Bowden, N., Arias, F., Yang, H. & Whitesides, G.M. Modeling of menisci and capillary forces from the millimeter to the micrometer size range. *J. Phys. Chem. B* **105**, 404-412 (2001).

S4. Vella, D., Mahadevan, L., The "Cheerios effect", *Am. J. Phys*, **73**(9), 817-825 (2005).